IEEE Access
Multidisciplinary ⋮ Rapid Review ⋮ Open Access Journal

Received 5 July 2022, accepted 15 July 2022, date of publication 22 July 2022, date of current version 4 August 2022.

Digital Object Identifier 10.1109/ACCESS.2022.3192128

RESEARCH ARTICLE

A Novel Broadband Microwave Lumped-Element Quadrature Hybrid MMIC

XI CHEN, ANYONG HU, JIANHAO GONG, RUOCHEN GU, WANGDONG HE, AND JUNGANG MIAO

School of Electronic and Information Engineering, Beihang University, Beijing 100191, China

Corresponding author: Anyong Hu (hu_anyong@buaa.edu.cn)

This work was supported by the National Natural Science Foundation Program of China under Grant 61731001.

ABSTRACT In this paper, a novel broadband lumped-element quadrature hybrid MMIC for interferometric correlation radiometer is proposed. First, the cause of the bandwidth limitation in the lumped-element branch-line coupler is analyzed, which is the two identical parallel branches have the same frequency response leading to reinforced resonance and narrow band. In order to reduce such unfavorable superposition effect, parallel branches with opposite frequency responses are used, which exhibits the characteristic similar to rat-race coupler. To realize a quadrature hybrid, a phase-shifting network is cascaded to the rat-race coupler, and the bandwidth is further extended by compensating the passband phase trend and optimizing the inter-stage matching of the two parts. Finally, to facilitate the application, the quadrature hybrid is combined with a variable gain amplifier to implement an integrated MMIC based upon 0.15 um GaAs pHEMT process, and the size of the hybrid part is 1.2×1.4 mm^2. Within the frequency range of 3.8∼8.5 GHz (75% fractional bandwidth), the amplitude and phase imbalance are less than 0.5 dB and 2.6°. All reflections and isolations are better than 16.4 dB. The measured results verify the design theory and illustrate that the lumped-element quadrature hybrid is suitable for compact broadband circuit applications.

INDEX TERMS Broadband, lumped-element, MMIC, phase-shifting network, quadrature hybrid, rat-race coupler.

I. INTRODUCTION

Quadrature hybrids are widely used passive components in microwave systems, which are mainly used for quadrature combining and division of signals. The application backgrounds of this paper are passive millimeter-wave imaging system and temperature measurement system, in which the core structure is an interferometric correlation radiometer [1]. Figure 1 shows a simplified block diagram of the radiometer, from which we can see that the quadrature hybrid is applied and plays an important role in the image-reject down conversion circuit [2], [3] and the 6-ports network of correlator [4]–[6]. For the radiometer, when the integration time is constant, broader bandwidth means better radiometric sensitivity. Moreover, the amplitude and phase imbalance of the hybrid is related to the image rejection ratio and correlation efficiency of the system. Therefore, the design challenge is to obtain a compact quadrature hybrid with 4 GHz bandwidth covering the C-band (4∼8 GHz, 67% fractional bandwidth) and low imbalance to meet the system requirements.

The conventional distributed planar hybrid circuit consists of multiple quarter-wavelength transmission lines (TLs) at the design frequency, which can easily obtain a fractional bandwidth (FBW) more than 60% [7]–[10]. However, the above distributed hybrids require a large circuit area, which makes it inconvenient for the application and integration in low-frequency circuits. Lumped-element hybrids are attractive for the small size and high integration, which are more suitable for the design of monolithic microwave integrated circuits (MMIC). The most intuitive circuit is to replace the TLs of branch line coupler with lumped LC network. Four kinds of hybrid based on this structure are introduced in [11], [12], but their FBW are about 10%.

The associate editor coordinating the review of this manuscript and approving it for publication was Chun-Hsing Li.

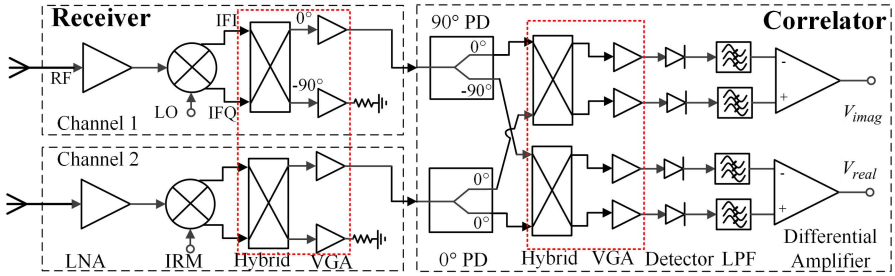

FIGURE 1. Diagram of the interferometric correlation radiometer.

In [13]–[17], the same design method as the planar circuit is adopted to connect two hybrids in series to improve bandwidth, so that measured FBW reaches 30%. [18] proposes a lumped-element coupler with resonant parallel LC, which measured FBW is 49%. Some of the state-of-the-art design methods have focused on impedance transformation or arbitrary coupling characteristics [19]–[21], while the bandwidth has not been improved. To sum up, the previously reported lumped-element quadrature hybrids cannot satisfy the bandwidth requirements of our radiometer application.

Therefore, a novel broadband and compact lumped-element quadrature hybrid circuit is proposed and designed. The main contributions of this paper are summarized as follows.

1) We analyze the existing lumped-element branch-line coupler and point out that the limitation of the bandwidth is attributed to two identical parallel branches with the same frequency response. Therefore, the idea of using parallel branches with opposite frequency response is proposed. Based on the rat-race coupler with the above characteristics of separate resonance points, a novel broadband quadrature hybrid circuit is constructed by cascading with the phase shift network.
2) In circuit design, the method of phase compensation and inter-stage matching optimization is adopted to ensure low phase imbalance while expanding bandwidth. This method is also applicable to other cascade configuration circuits.
3) Compared with previously reported lumped-element works, the bandwidth of proposed quadrature hybrid is significantly expanded to 75% without occupying more chip area ($0.07\lambda g \times 0.08\lambda g$). The proposed quadrature hybrid is very suitable for broadband and highly integrated circuit applications.

The rest of this paper is organized as follows. In Section II, the bandwidth is analyzed and the proposed circuit is proved to be a quadrature hybrid. Section III illustrates the lumped-element hybrid design approach, including presenting simplified schematic and full-wave simulation results. Section IV introduces the design and simulation of a variable gain amplifier (VGA), which is cascaded with the hybrid to form a C-band integrated chip, as shown in the red box in Figure 1. The modular measurement setup of quadrature hybrid integrated MMIC is given in Section V, and the measurement results are compared with the simulation and the previously reported works. Finally, Section VI summarizes the results and conclusions of this paper.

II. ANALYSIS OF THE BROADBAND LUMPED-ELEMENT QUADRATURE HYBRID

The design of lumped-element circuits is usually based on multistage symmetric high-pass (HP) or low-pass (LP) LC units. The LC units can be obtained by using the ABCD matrix equivalent to that of TLs [11], [22]. Taking the π-type LP LC unit as an example, the LC unit and TL are expressed as:

$$\begin{bmatrix} A & B \\ C & D \end{bmatrix}_{low-pass} = \begin{bmatrix} 1-\omega^2 CL & j\omega L \\ j\omega C\left(2-\omega^2 CL\right) & 1-\omega^2 CL \end{bmatrix} \quad (1)$$

$$\begin{bmatrix} A & B \\ C & D \end{bmatrix}_{TL} = \begin{bmatrix} cos\Phi & jZ_r sin\Phi \\ jY_r sin\Phi & cos\Phi \end{bmatrix} \quad (2)$$

where Z_r and Φ are the characteristic impedance and insertion phase of the TL, respectively. When an LC unit in a cascaded configuration with a small insertion phase is adopted, its characteristics are closer to a TL, so broadband are easier to obtain, as shown in Figure 2. However, the previously published lumped-element couplers based on this structure have not been able to achieve a bandwidth comparable to the distributed-element circuits, which is worth analyzing.

A. BANDWIDTH ANALYSIS OF LUMPED-ELEMENT COUPLER

The even-odd mode is an effective method to analyze symmetric circuits. By adopting this method, as shown in Figure 3(a), the traditional ring structure branch-line coupler can be divided into the combination of TL and open or short stubs. Figure 3(b) is the form of the +45° stub in even mode and odd mode represented by π-type LP LC unit, and their values are expressed as

$$L_{L\pi} = \frac{Z_r sin\left(\Phi\right)}{\omega_c}, \quad C_{L\pi} = \frac{1-cos\left(\Phi\right)}{Z_r \omega_c sin\left(\Phi\right)} \quad (3)$$

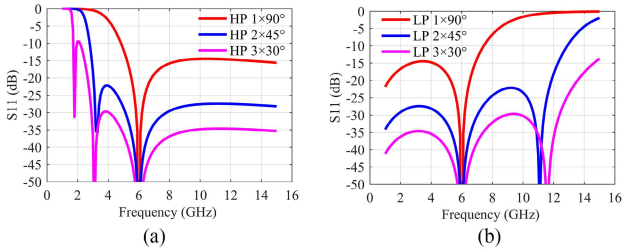

FIGURE 2. Comparison of cascaded LP/HP LC units with different insertion phases (1-stage 90° LC unit, 2-stage 45° LC units, and 3-stage 30° LC units).

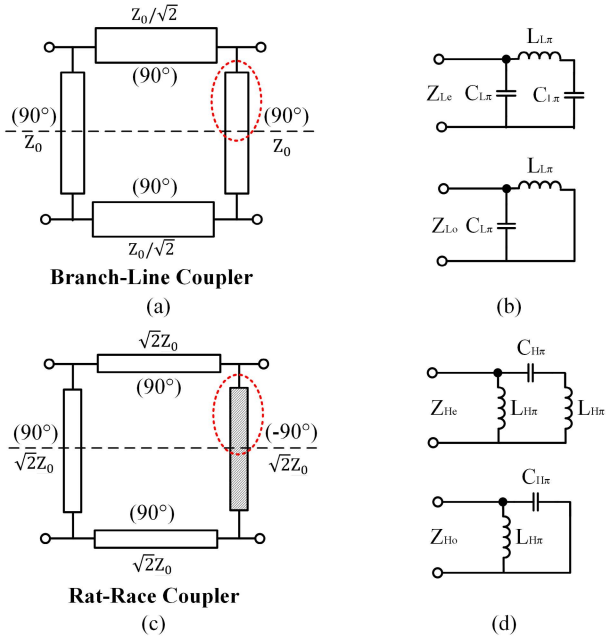

FIGURE 3. (a) Branch-line coupler block diagram. (b) Lumped-element +45 ° stub in even mode and odd mode. (c) Rat-race coupler block diagram. (d) Lumped-element −45 ° stub in even mode and odd mode.

The corresponding impedance expressions are:

$$Z_{Le} = jZ_r \frac{\left(\sqrt{2}-1\right)x^2 - \sqrt{2}}{\left(2\sqrt{2}-3\right)x^3 + \left(4-2\sqrt{2}\right)x}, \quad x = \frac{\omega}{\omega_c} \tag{4}$$

$$Z_{Lo} = jZ_r \frac{x}{\left(1-\sqrt{2}\right)x + \sqrt{2}}, \quad x = \frac{\omega}{\omega_c} \tag{5}$$

where $\omega_c = 2\pi f_c$, f_c is the center frequency. It is found that when $f = 1.85 f_c$, Z_{Le} and Z_{Lo} are 0 and ∞ respectively, which means that both LP LC units affect the transmission characteristics at 1.85 f_c, and lead to reinforced resonance, limiting the bandwidth. In order to reduce such unfavorable superposition effect at same frequency, we thought of using two parallel stubs with opposite frequency responses, which happens to be the case with rat-race coupler [22]–[25], and one of the stubs can be replaced by −45 ° HP LC unit, as shown in Figure 3(c) (d). The LC value and the impedance

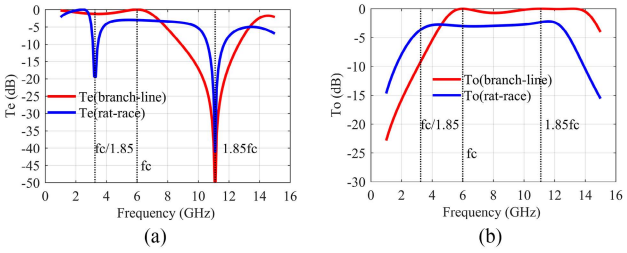

FIGURE 4. (a) Even mode transmission characteristics of branch-line coupler and rat-race coupler. (b) odd mode transmission characteristics.

of the stub are:

$$L_{H\pi} = \frac{Z_r sin\,(\Phi)}{\omega_c\,(1 - cos\,(\Phi))}, \quad C_{H\pi} = \frac{1}{Z_r \omega_c sin\,(\Phi)} \tag{6}$$

$$Z_{He} = jZ_1 \frac{\sqrt{2}\,x^3 - \left(\sqrt{2}-1\right)x}{\left(4-2\sqrt{2}\right)x^2 + \left(2\sqrt{2}-3\right)}, \quad x = \frac{\omega}{\omega_c} \tag{7}$$

$$Z_{Ho} = jZ_1 \frac{x}{-\sqrt{2}\,x + \left(\sqrt{2}-1\right)}, \quad x = \frac{\omega}{\omega_c} \tag{8}$$

In even mode, the ±45° LC units resonate at 1.85 f_c and $f_c/1.85$ respectively without affecting the passband. From the simulation results in Figure 4(a), it can be clearly seen that the even mode transmission characteristics of the branch-line coupler has intensified losses around 1.85 f_c, while the rat-race coupler has band-pass characteristics. In odd mode, The LC units also resonates at different frequencies, showing a low-loss passband between the two frequencies, as shown in Figure 4(b). That is to say, when using the same design method, the rat-race coupler has a larger bandwidth characteristic.

If the TL of each arm is changed to a three-stage cascaded LC unit, the same method is used to calculate that the resonant frequency of limiting the bandwidth becomes 1.93 f_c and $f_c/1.93$. The quantity of lumped elements is increased by 50%, but the bandwidth is only increased by approximately 6%, so the two-stage structure is more reasonable.

B. A NOVEL BROADBAND LUMPED-ELEMENT QUADRATURE HYBRID

According to the above analysis, although the rat-race coupler based on two-stage cascade configuration LC units has bandwidth advantages, its 0° /180° phase difference cannot be used for sideband separation of the image-reject mixer and the quadrature synthesis of the six-port network, which is inconsistent with applications.

Therefore, a novel broadband lumped-element quadrature hybrid is proposed by connecting different ±45° LP/HP LC units at ports. As shown in Figure 5, the connected LC units can be regarded as a phase-shifting network, and the phase difference can be changed through different combinations. The ABCD matrix expressions of even mode and odd mode

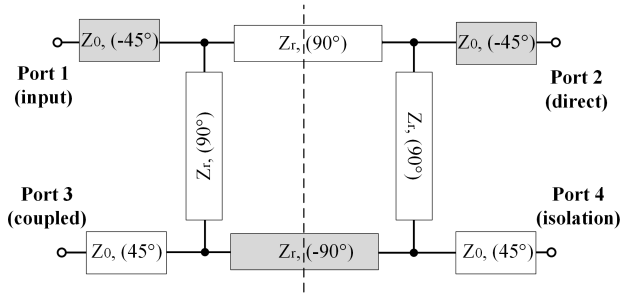

FIGURE 5. Schematic diagram of the proposed quadrature hybrid.

and S parameters calculated from them are as follows:

$$\begin{bmatrix} A & B \\ C & D \end{bmatrix}_{even} = \begin{bmatrix} 0 & (\sqrt{2}+1)j \\ (\sqrt{2}-1)j & 0 \end{bmatrix} \tag{9}$$

$$\begin{bmatrix} A & B \\ C & D \end{bmatrix}_{odd} = \begin{bmatrix} 0 & (\sqrt{2}-1)j \\ (\sqrt{2}+1)j & 0 \end{bmatrix} \tag{10}$$

$$\Gamma_e = \frac{1}{\sqrt{2}}, \quad T_e = -\frac{1}{\sqrt{2}}j, \quad \Gamma_o = -\frac{1}{\sqrt{2}},$$
$$T_o = -\frac{1}{\sqrt{2}}j \tag{11}$$

$$S_{11} = \frac{1}{2}\Gamma_e + \frac{1}{2}\Gamma_o = 0 \tag{12}$$

$$S_{21} = \frac{1}{2}\Gamma_e - \frac{1}{2}\Gamma_o = \frac{1}{\sqrt{2}} \tag{13}$$

$$S_{31} = \frac{1}{2}T_e + \frac{1}{2}T_o = -\frac{1}{\sqrt{2}}j \tag{14}$$

$$S_{41} = \frac{1}{2}T_e - \frac{1}{2}T_o = 0 \tag{15}$$

Using ports 2, 3, and 4 as sources in turn, the complete scattering matrix of the circuits can be obtained:

$$[S] = -\frac{\sqrt{2}}{2}j \begin{bmatrix} 0 & j & 1 & 0 \\ j & 0 & 0 & 1 \\ 1 & 0 & 0 & j \\ 0 & 1 & j & 0 \end{bmatrix} \tag{16}$$

This result can prove that the proposed circuit is completely equivalent to a quadrature hybrid.

III. QUADRATURE HYBRID CIRCUIT DESIGN METHOD AND BANDWIDTH EXPANSION

The schematic diagram of the proposed lumped-element quadrature hybrid based on multistage LC units is shown in Figure 6. The corresponding LC values of this basic structure is expressed in the form of the inserted phase as follows:

$$L_1 = \frac{Z_r sin(\Phi)}{(1-cos(\Phi))\omega_c}, \quad C_1 = \frac{1}{Z_r \omega_c sin(\Phi)},$$
$$Z_r = \sqrt{2}Z_0 \tag{17}$$
$$L_2 = \frac{Z_r sin(\Phi)}{\omega_c}, \quad C_2 = \frac{1-cos(\Phi)}{Z_r \omega_c sin(\Phi)},$$
$$Z_r = \sqrt{2}Z_0 \tag{18}$$

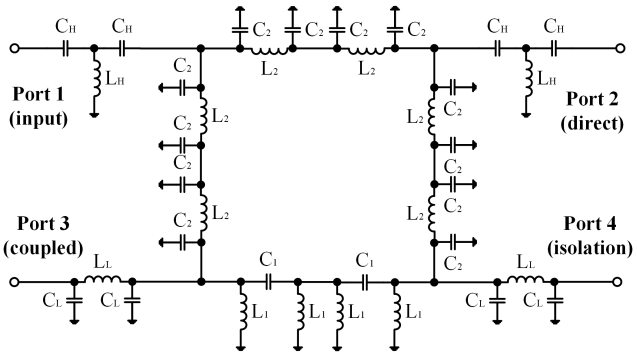

FIGURE 6. Schematic diagram of lumped-element quadrature hybrid constructed by rat-race coupler with two-stage LC units on each arm and HP/LP phase-shifting network.

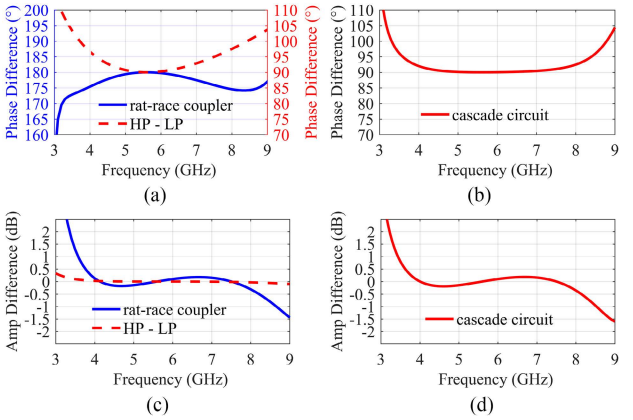

FIGURE 7. (a) Phase difference of rat-race coupler and HP/LP network. (b) Phase difference of quadrature hybrid. (c) Amplitude difference of rat-race coupler and HP/LP network. (d) Amplitude difference of quadrature hybrid.

$$L_H = \frac{Z_0}{\omega_c sin(\Phi)}, \quad C_H = \frac{sin(\Phi)}{Z_0 \omega_c (1-cos(\Phi))} \tag{19}$$

$$L_L = \frac{Z_0 sin(\Phi)}{\omega_c}, \quad C_L = \frac{1-cos(\Phi)}{Z_0 \omega_c sin(\Phi)} \tag{20}$$

where all Φ are 45°, because the arms of the rat-race coupler in the middle ring structure are two-stage cascaded LC units.

A. LOW PHASE IMBALANCE CHARACTERISTIC

When analyzing rat-race coupler and phase-shifting network separately, we select the center frequency of 5.6 GHz as an example. The lumped-element values are calculated according to (17) ∼ (20): $C_1 = 0.57$ pF, $L_1 = 4.85$ nH, $C_2 = 0.17$ pF, $L_2 = 1.42$ nH, $C_L = 0.24$ pF, $L_L = 1$ nH, $C_H = 1.37$ pF, $L_H = 2.01$ nH. It can be seen from Figure 7(a) that the both phase difference curves are not flat in broadband, and the deviation from the center frequency increases with the expansion of the bandwidth. The maximum phase difference variation of the two curves in the band is 5.5° and 7.5°. However, the trend of the phase difference curve between the HP and LP phase-shifting network is opposite to the characteristics of the rat-race coupler. This implies that the

TABLE 1. Performance analysis of the proposed hybrid.

α	C_1 (pF)	L_1 (nH)	C_2 (pF)	L_2 (nH)	Passband Ripple (dB)	Return Loss (dB)	Amplitude Imbalance (dB)	Phase Imbalance (°)	Bandwidth (GHz)	Fractional Bandwidth
1.0	0.57	4.85	0.17	1.42	0.34	> 12.5	< 0.18	< 2.2	3.96~7.68	64%
0.9	0.63	4.37	0.19	1.28	0.50	> 12.7	< 0.27	< 2.7	3.80~7.98	71%
0.8	0.71	3.88	0.21	1.14	0.55	> 13.1	< 0.38	< 3.2	3.72~8.14	75%
0.7	0.81	3.40	0.24	1.00	0.65	> 9.30	< 0.58	< 4.2	3.62~8.28	78%

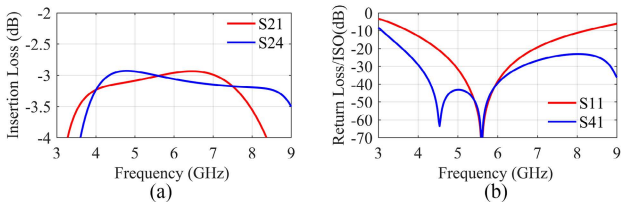

FIGURE 8. Preliminary simulation results of the quadrature hybrid circuit. (a) Insertion loss. (b) Return loss and isolation.

phase-shifting network is not arbitrarily distributed at each port of the coupler, and a small phase difference variation can be obtained when the layout design makes the phases of the two parts compensate for each other. After the two parts are cascaded to form a complete quadrature hybrid circuit, the phase difference simulation result is 90° ∼92.2°, as shown in Figure 7(b). Phase compensation is also an important idea for subsequent circuit simplification and layout optimization.

As a ±45° LC unit, the HP/LP network has a very flat amplitude characteristic in broadband, so the amplitude difference of the quadrature hybrid mainly depends on the rat-race coupler, which is less than ±0.4 dB, as depicted in Figure 7(c) and (d).

B. BROADBAND CHARACTERISTIC

As shown in Figure 8, in the preliminary simulation results of the hybrid, the bandwidth can reach 3.9∼7.7 GHz (64% FBW), which is already wider than the previously reported lumped-element quadrature hybrids. Moreover, according to the derivation in Section II (16) and the simulation result of return loss, for the center frequency f_c, the circuit port is completely matched with Z_0. In order to analyze the relationship between bandwidth and matching, we introduce a coefficient α to change the impedance on each arm of rat-race coupler, $Z_r' = \alpha\sqrt{2}Z_0$. The f_c is still selected as 5.6 GHz, and the impedance of HP/LP networks does not change with α.

As can be seen from Figure 9 and Table 1, the bandwidth is effectively further increased from 64% to 78% by compromising return loss and passband ripple. The amplitude difference between two ports is defined as the amplitude imbalance, while the phase difference deviating by 90° is defined as the phase imbalance. Their changes are also within the acceptable range.

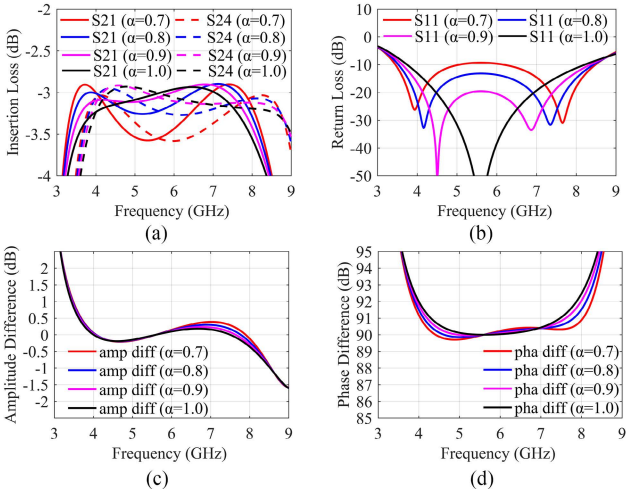

FIGURE 9. Relationship between α and hybrid characteristics. (a) α and passband ripple. (b) α and return loss. (c) α and amplitude difference. (d) α and phase difference.

C. QUADRATURE HYBRID SCHEMATIC SIMPLIFICATION AND LAYOUT FULL-WAVE SIMULATION

The lumped elements in the quadrature hybrid circuit can be further simplified before MMIC layout design. First, the parallel capacitors or inductors in each arm can be combined. Second, the parallel L_1 and C_2 of two adjacent arms resonate at the central frequency, which can be equivalent to an open circuit. After removing L_1C_2, as shown in Figure 10(a), only the center frequency is not affected, the phase difference in the broadband becomes a downward trend with the increase of frequency and the phase imbalance increases to 10°. However, using the idea of phase compensation, the phase-shifting network in the circuit provides us with the possibility of adjustment. According to the HP/LP phase difference curve in Figure 7(a), the slope in band can appear in the opposite direction by tuning the center frequency, even adjusting the value of Φ if necessary. For example, when L_1C_2 is removed and HP/LP network is designed as center frequency of 4.7 GHz, the optimized phase difference becomes flat again, as shown in Figure 10(b).

Second, the port relationship of the proposed quadrature hybrid is different from that of the traditional hybrid. For the convenience of application, the port position is shifted according to the symmetry of the circuit structure, and avoid

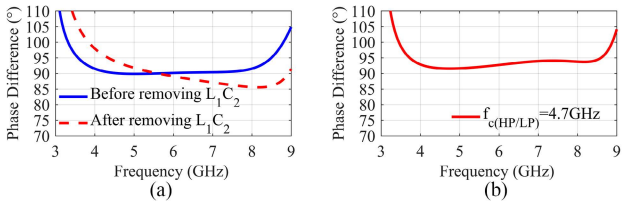

FIGURE 10. Phase compensation in schematic simplification. (a) Comparison on removing L_1 and C_2. (b) Optimized phase difference.

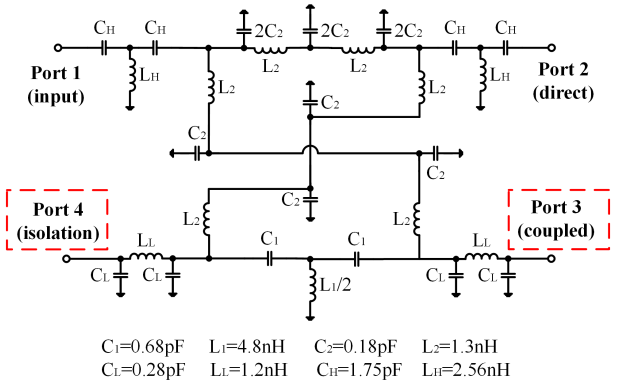

FIGURE 11. Final schematic of the quadrature hybrid and the values of lumped-elements.

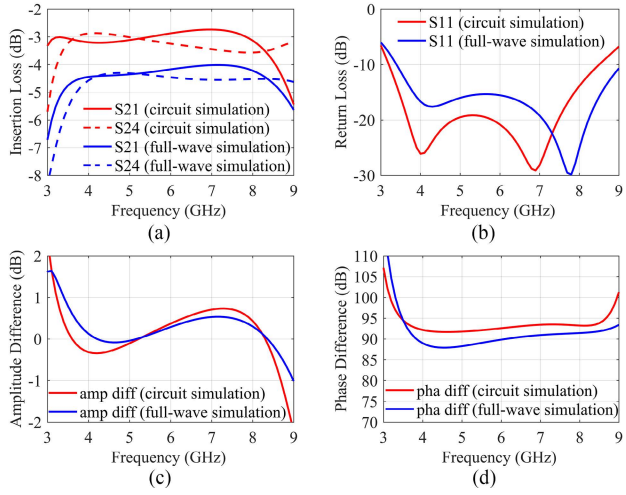

FIGURE 12. Comparison on circuit simulation and full-wave simulation results.

the lines crossing by using an air bridge. The isolation of the air bridge part is greater than 35 dB at this frequency, so it does not affect the overall performance. After adjustment, the input port (port 1) and isolation port (port 4) are on the same side, and the direct port (port 2) and coupled port (port 3) are on the other side, which facilitates interconnection with adjacent circuits. The final schematic and the values of lumped elements are shown in Figure 11.

After optimization, the proposed quadrature hybrid still has 28 lumped elements, which is a relatively large number. Therefore, it is necessary to attach importance to the chip

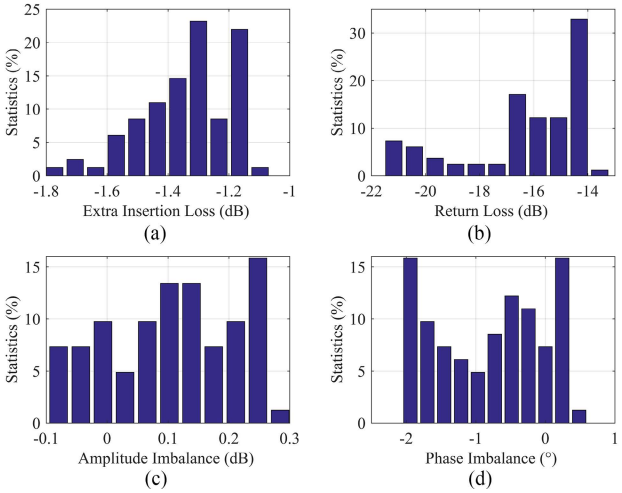

FIGURE 13. Yield analysis of the proposed quadrature hybrid. (a) Extra insertion loss. (b) Return loss. (c) Amplitude imbalance. (d) Phase imbalance.

area, extra insertion loss and the error caused by process stability. In the MMIC layout design, the HP unit in the phase-shifting network adopts a T-type, while the LP unit is a π-type, which is to reduce the number of inductors that occupy more area, so that the MMIC is compact. Several shunt capacitors at the air bridge are not combined, but evenly arranged in the circuit. This maintains symmetry for the physical structure to reduce imbalance. The parasitics of the lines connecting the lumped-element are considered in the full-wave simulation. In Figure 12, the extra insertion loss of the full-wave simulation is about 1.3 dB, and the other results are close to the circuit simulation.

Yield simulation is performed to analyze the sensitivity of the circuit to process and temperature variations. The probability distribution functions of yield variables provided by the foundry are used for simulation. Statistics are performed on each parameter in the range of 4 to 8 GHz, as shown in Figure 13, where the ordinate is the proportion in 500 times simulations. It is shown that the variation range of the extra insertion loss is 1.1∼1.8 dB, the return loss is always lower than −13 dB, and the amplitude and phase imbalance are less than 0.3 dB and 2°. The yield simulation results demonstrate that the performance varies within a predictable range with process and temperature.

IV. VARIABLE GAIN AMPLIFIER DESIGN

Referring to Figure 1, it can be seen that in the receiver and correlator, the two output ports of the quadrature hybrid are each connected to an amplifier. Therefore, we propose to design the hybrid and amplifier cascade as an integrated chip for the convenience of application. However, the amplifier plays different roles in these two places.

In the receiver, the amplifier is used to adjust the gain to ensure the consistency of the different receiving channels. In addition, only one sideband is required in the image-reject down conversion, and the image sideband is often

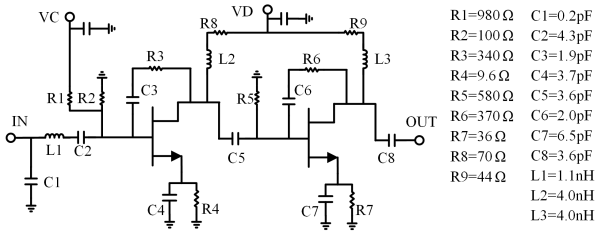

FIGURE 14. Schematic diagram of the VGA.

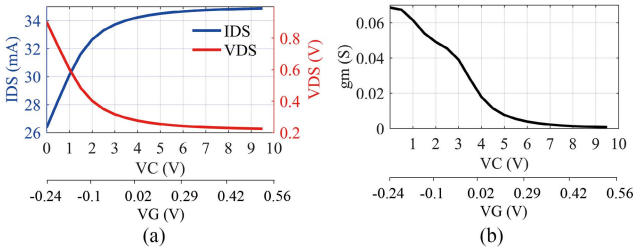

FIGURE 15. DC characteristics of the VGA stage. (a) IDS and VDS changes with VC or VG. (b) gm changes with VC or VG.

matched and absorbed by a resistive load. That is to say, only one amplifier is needed in a particular case. Therefore, an idea is put forward that when the amplifier is not powered, its input terminal is also matched, which not only saves the power consumption, but also eliminates the need for external matching loads. In the correlator, the detectors tend to be poorly matched in the broadband range. To prevent the reflected signal into the hybrid and affecting its balance, the amplifier is used to provide high reverse isolation. To sum up, the amplifier is a VGA, and it maintains good return loss and isolation when the gain changes, without pursuing high gain. the VGA is made of two 4×50 μm common-source transistors, in which the first stage provides variable gain and the second stage is constant gain. Firstly, both the two-stage adopts the self-bias scheme to avoid negative DC power supply while voltage dividing resistors are used at drain, leaving only one +3V power supply pad. In addition, in order to ensure the flatness in the band when the gain changes, RC feedback topology is used. The schematic diagram is shown in Figure 14. The simulated small-signal gains of the two stages are 7dB and 10dB, respectively.

The VGA stage design is based on a variable trans-conductance (gm) topology [26]. The trans-conductance of active devices is controlled through the variation of external DC control voltage (VC), so that the gain changes accordingly. In this design, the VC is added to the gate of the transistor after using voltage dividing resistors (R1 and R2). Since the circuit adopts a self-biasing structure, the VC can be a positive voltage, and no additional active devices are required [27]. Figure 15 shows the DC characteristics of the VGA stage. It is evident that VGS changes with the VC, while gm varies from high to low. The maximum gain is obtained around VC = 0V, when gm is maximum. With the increase of VC, the gm curve becomes flat, which means that further gain variation cannot be achieved.

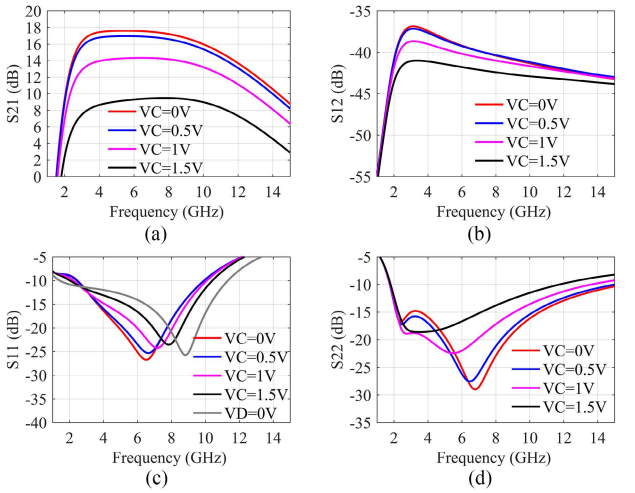

FIGURE 16. S-parameter full-wave simulation results of VGA. (a) Gain. (b) reverse isolation. (c) input return loss. (d) output return loss.

Figure 16 shows the full-wave simulation results of the VGA chip when the VC changes from 0 to 1.5V. The gain varies from 17 to 9 dB and is flat in the 4∼8 GHz range. As the VC ascends, the gain variation range can continue to increase, but since the VGA is only used to adjust the consistency of channels, the current variation range of gain is sufficient. The reverse isolation is greater than 37 dB. The return loss of the input port remains below −12 dB, even if there is no VD power supply. This is because the voltage dividing resistor R2 is also used as part of the matching circuit, making a trade-off between matching and gain.

V. IMPLEMENTATION AND MEASUREMENTS

The quadrature hybrid integrated MMIC process based upon a standard 0.15 um GaAs pHEMT. The microphotograph of the MMIC is shown in Figure 17, in which the quadrature hybrid is on the left and the two VGAs are on the right, with the RF and DC ports located at the edge of the MMIC. The overall size is $2.3 \times 2\text{mm}^2$, of which the quadrature hybrid part occupies $1.2 \times 1.4\text{mm}^2$.

Probe measurement can best show the performance of the MMIC itself, but the spacing between the ports is very small and cannot be connected with all probes at the same time. Therefore, we assemble the MMIC into a module with bonding wires. Although there are parasitic and loss of the transmission line, the measurement results reflect the real application state. The device under test (DUT) and the measurement environment are shown in Figure 18. The vector network analyzer (N5227B) is used to measure S parameters.

The DUT is measured under the normal operating condition when VD = 3 V, VC = 0 V, and compare with the simulation result to evaluate the quadrature hybrid. In Figure 19 (a) and (b), the bandwidth range that we are most concerned about is 3.8∼8.5 GHz (FBW 75%). Within this frequency band, the gain is about 3 dB lower than the simulation, which can be understood as the loss introduced by the bonding wires, PCB transmission line and

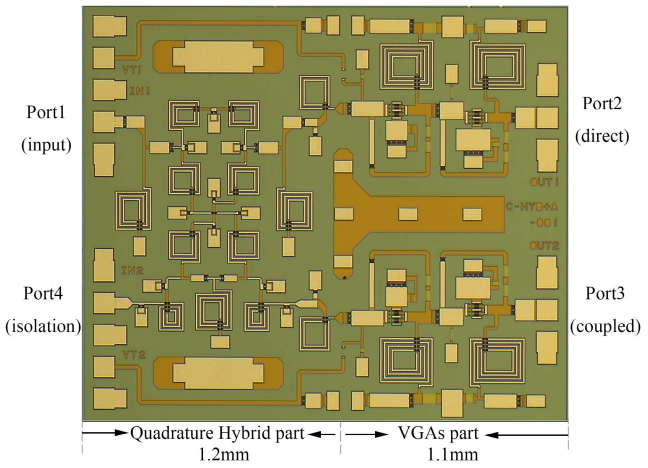

FIGURE 17. Microphotograph of the quadrature hybrid and VGA integrated MMIC.

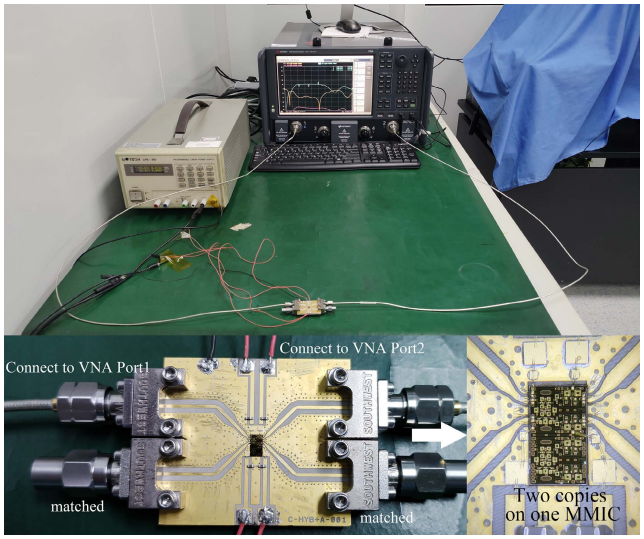

FIGURE 18. Modular measurement set-up.

coaxial connectors during modular measurement. However, the overall trend is close to the simulation results, and the passband ripple is less than 0.7 dB. S11 in Figure 19 (c) reflects the input return loss of the quadrature hybrid, which is less than −16.4 dB. S22 shows that the output return loss of the VGA is less than −22 dB. Both the measured results are better than the simulation. Figure 19 (d) presents the isolation of the hybrid S14 and the reverse isolation S12. The reverse isolation greater than 40 dB meets the application requirements in the correlator. The amplitude and phase imbalance of two different paths are compared in Figure 19 (e) and (f). When the direct port (port 2) is used as the output port, the amplitude and phase imbalance is 0.5 dB and 2.6°, respectively, while the coupled port (port 3) corresponds to 0.4 dB and 1.8°.

Table 2 lists the comparison with other quadrature hybrids reported in recent years. Due to the difference in the process

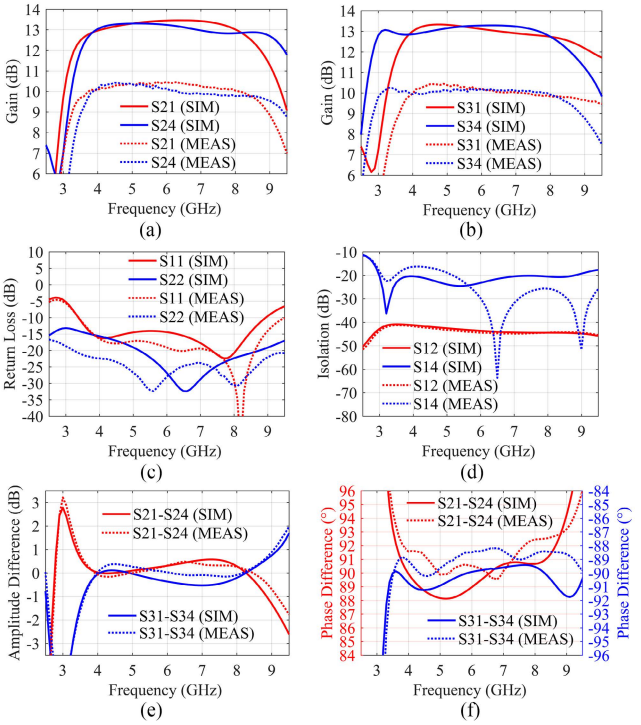

FIGURE 19. Comparison of modular measurement and simulation of quadrature hybrid integrated MMIC.

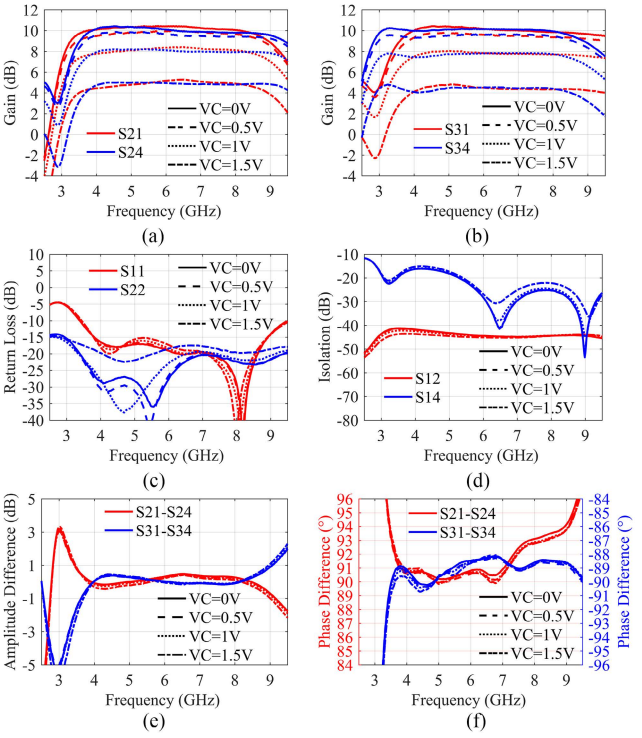

FIGURE 20. Modular measurement results of quadrature hybrid integrated MMIC with VC changing.

or substrate of various circuits, the guided wavelength (λ_g) is used as the unit of size. It is obvious that the size of lumped-element hybrids is significantly decreased. The bandwidth of

TABLE 2. Comparison with the previously reported 3dB quadrature hybrids.

Reference	Architecture	Tech.	Amplitude Imbalance (dB)	Phase Imbalance (°)	Circuit size ($\lambda_g \times \lambda_g$)	Fractional Bandwidth
[9]2021	Distributed	PCB	1	5	0.3×0.5	51%
[10]2022	Distributed	PCB	1.5	5	0.4×0.7	54%
[14]2007	Lumped	GaAs MMIC	0.7	3.7	0.1×0.04	18.2%
[15]2003	Lumped	SMD	1	5	0.04×0.02	38%
[18]2019	Lumped	GaN MMIC	1.2	6	0.2×0.09	49%
[20]2020	Lumped	GaAs MMIC	1	2.5	0.03×0.02	17.4%
[21]2022	Lumped	SMD	0.5	5	0.06×0.06	25%
This work	Lumped	GaAs MMIC	0.5	2.6	0.07×0.08	75%

the proposed quadrature hybrid is greatly improved in the limited chip area, while maintaining a low phase imbalance in the band.

Further, the control voltage VC was adjusted from 0 to 1.5 V, and the effects on S-parameters and imbalance were measured and observed. It can be seen from Figure 20 that the gain changes from 10.6 dB to about 5 dB, and at the same time, the other S-parameters and the imbalance are almost unchanged. It shows that the quadrature hybrid and the VGA have excellent inter-stage matching, so that the adjustment of the VGA has no effect on the hybrid.

VI. CONCLUSION

In this paper, a novel lumped-element quadrature hybrid is proposed and demonstrated. In the circuit design, the broadband characteristics is analyzed, and it is cascaded with a VGA chip and implemented as a C-band integrated MMIC based on the GaAs process. The measurement results show that the quadrature hybrid has 75% FBW, less than 0.5 dB and 2.6° imbalance, and the circuit area only occupies 1.2mm × 1.4mm ($0.07\lambda g \times 0.08\lambda g$), which is very suitable for applications in broadband and high-integration circuits.

REFERENCES

[1] M. Martàn-Neira, D. M. LeVine, Y. Kerr, N. Skou, M. Peichl, A. Camps, I. Corbella, M. Hallikainen, J. Font, J. Wu, S. Mecklenburg, and M. Drusch, "Microwave interferometric radiometry in remote sensing: An invited historical review," *Radio Sci.*, vol. 49, no. 6, pp. 415–449, Jun. 2014, doi: 10.1002/2013RS005230.

[2] S. Zhang, L. Sun, J. Wen, and J. Liu, "A 48 GHz-78 GHz MMIC sub-harmonic pumped image rejection mixer," presented at the IEEE Int. Conf. Semiconductor Electron. (ICSE), Kuala Lumpur, Malaysia, Aug. 2014.

[3] P. Yan, W. Hong, and J. Chen, "Design of monolithic image rejection mixer," presented at the Int. Symp. Signals, Syst. Electron., Nanjing, China, Sep. 2010.

[4] C. Wang, X. Xin, B. Liang, Z. Li, and J. Miao, "Quadrature errors and DC offsets calibration of analog complex cross-correlator for interferometric passive millimeter-wave imaging applications," *Sensors*, vol. 18, no. 2, p. 677, Feb. 2018, doi: 10.3390/s18020677.

[5] S. Padin, J. K. Cartwright, M. C. Shepherd, J. K. Yamasaki, and W. L. Holzapfel, "A wideband analog correlator for microwave background observations," *IEEE Trans. Instrum. Meas.*, vol. 50, no. 5, pp. 1234–1240, Oct. 2001, doi: 10.1109/19.963190.

[6] A. Koelpin, F. Lurz, S. Linz, S. Mann, C. Will, and S. Lindner, "Six-port based interferometry for precise radar and sensing applications," *Sensors*, vol. 16, no. 10, p. 1556, Sep. 2016, doi: 10.3390/s16101556.

[7] U. Dilshad, C. Chen, X. Chen, and J. Miao, "Broadband quadrature hybrid for image rejection in millimeter-wave receivers," presented at the 16th Int. Bhurban Conf. Appl. Sci. Technol. (IBCAST), Islamabad, Pakistan, Jan. 2019.

[8] R. Smolarz, K. Wincza, and S. Gruszczynski, "Chebyshev-response branch-line couplers with enhanced bandwidth and arbitrary coupling level," *Electronics*, vol. 9, no. 11, p. 1828, Nov. 2020, doi: 10.3390/electronics9111828.

[9] M. Liu and F. Lin, "Two-section broadband couplers with wide-range phase differences and power-dividing ratios," *IEEE Microw. Wireless Compon. Lett.*, vol. 31, no. 2, pp. 117–120, Feb. 2021, doi: 10.1109/LMWC.2020.3041256.

[10] L. Pan, Y. Wu, W. Wang, Y. Zheng, and Y. Liu, "A symmetrical broadband tight-coupled directional coupler with high directivity using three-folded-coupled lines," *IEEE Trans. Circuits Syst. II, Exp. Briefs*, early access, Apr. 21, 2022, doi: 10.1109/TCSII.2022.3169160.

[11] L.-H. Lu, S. Mohammadi, G. E. Ponchak, P. Bhattacharya, and L. P. B. Katehi, "Design and implementation of micromachined lumped quadrature (90°) hybrids," in *IEEE MTT-S Int. Microw. Symp. Dig.*, Phoenix, AZ, USA, May 2001, pp. 1285–1288.

[12] M. Beigizadeh, R. Dehghani, and A. Nabavi, "Analysis and design of a lumped-element hybrid coupler using limited quality factor of components," *AEU Int. J. Electron. Commun.*, vol. 82, pp. 312–320, Dec. 2017, doi: 10.1016/j.aeue.2017.09.001.

[13] Y.-C. Chiang and C.-Y. Chen, "Design of a wide-band lumped-element 3-dB quadrature coupler," *IEEE Trans. Microw. Theory Techn.*, vol. 49, no. 3, pp. 476–479, Mar. 2001, doi: 10.1109/22.910551.

[14] J. A. Hou and Y. H. Wang, "A compact quadrature hybrid based on high-pass and low-pass lumped elements," *IEEE Microw. Wireless Compon. Lett.*, vol. 17, no. 8, pp. 595–597, Aug. 2007, doi: 10.1109/LMWC.2007.901775.

[15] W.-S. Tung, H.-H. Wu, and Y.-C. Chiang, "Design of microwave wide-band quadrature hybrid using planar transformer coupling method," *IEEE Trans. Microw. Theory Techn.*, vol. 51, no. 7, pp. 1852–1856, Jul. 2003, doi: 10.1109/TMTT.2003.814311.

[16] V. K. Velidi, A. V. G. Subramanyam, and V. V. Srinivasan, "Improved bandwidth via-free lumped-element quadrature hybrid couplers," presented at the IEEE Int. Microw. RF Conf. (IMaRC), Bangalore, India, Feb. 2014.

[17] Q. Wang, S. He, Y. Zhu, N. Wang, X. Li, P. Chen, L. Huang, Z. Cai, and B. Zhou, "Broadband lumped-element quadrature hybrid for intermediate frequency applications," presented at the Cross Strait Quad-Regional Radio Sci. Wireless Technol. Conf. (CSQRWC), Xuzhou, China, Jul. 2018.

[18] O. Kazan, O. Memioglu, F. Kocer, A. Gundel, and C. Toker, "A lumped-element wideband 3-dB quadrature hybrid," *IEEE Microw. Wireless Compon. Lett.*, vol. 29, no. 6, pp. 385–387, Apr. 2019, doi: 10.1109/LMWC.2019.2911648.

[19] D. Wang, J. Song, X. Li, Q. Qin, and L. Sun, "Design of wideband and compact lumped-element couplers for 5G communication," presented at the IEEE 6th Int. Conf. Comput. Commun. (ICCC), Chengdu, China, Dec. 2020.
[20] H. Ahn, I. Nam, and O. Lee, "An integrated lumped-element quadrature coupler with impedance transforming," *IEEE Microw. Wireless Compon. Lett.*, vol. 30, no. 2, pp. 152–155, Jan. 2020, doi: 10.1109/LMWC.2019.2963178.
[21] Z. Chen, Y. Wu, Y. Yang, and W. Wang, "A novel unequal lumped-element coupler with arbitrary phase differences and arbitrary impedance matching," *IEEE Trans. Circuits Syst. II, Exp. Briefs*, vol. 69, no. 2, pp. 369–373, Jun. 2022, doi: 10.1109/TCSII.2021.3093528.
[22] T.-M. Shen, C.-R. Chen, T.-Y. Huang, and R.-B. Wu, "Design of lumped rat-race coupler in multilayer LTCC," presented at the Asia–Pacific Microw. Conf., Singapore, Dec. 2009.
[23] I. A. Mocanu, "Compact dual band ring coupler using miniaturized metamaterial left-handed impedance inverters," *IEEE Access*, vol. 9, pp. 86119–86191, 2021, doi: 10.1109/ACCESS.2021.3089600.
[24] L. Chang and T.-G. Ma, "Dual-mode branch-line/rat-race coupler using composite right-/left-handed lines," *IEEE Microw. Wireless Compon. Lett.*, vol. 27, no. 5, pp. 449–451, Apr. 2017, doi: 10.1109/LMWC.2017.2690851.
[25] H. Okabe, C. Caloz, and T. Itoh, "A compact enhanced-bandwidth hybrid ring using an artificial lumped-element left-handed transmission-line section," *IEEE Trans. Microw. Theory Techn.*, vol. 52, no. 3, pp. 798–804, Mar. 2004, doi: 10.1109/TMTT.2004.823541.
[26] K. W. Kobayashi, K. T. Ip, A. K. Oki, D. K. Umemoto, S. Claxton, M. Pope, and J. Wiltz, "GaAs HBT 0.75–5 GHz multifunctional microwave-analog variable gain amplifier," *IEEE J. Solid-State Circuits*, vol. 29, no. 10, pp. 1257–1261, Oct. 1994, doi: 10.1109/4.315212.
[27] M. A. Masud, H. Zirath, and M. Kelly, "A 45-dB variable-gain low-noise MMIC amplifier," *IEEE Trans. Microw. Theory Techn.*, vol. 54, no. 6, pp. 2848–2855, Jun. 2006, doi: 10.1109/TMTT.2006.875453.

XI CHEN received the B.S. degree from Shenyang Aerospace University, Shenyang, China, in 2013, and the M.S. degree from the School of Electronics and Information Engineering, Beihang University, Beijing, China, in 2018, where he is currently pursuing the Ph.D. degree. His current research interests include monolithic microwave integrated circuits design based on gallium arsenide and RF/microwave circuit design.

ANYONG HU was born in Loudi, Hunan, China, in 1980. He received the B.S. degree in telecommunication engineering from the National University of Defense and Technology, in 2003, and the Ph.D. degree in signal processing from Beihang University, in 2009. He was a Postdoctoral Researcher for passive millimeter imaging with the Electromagnetic Laboratory, Beihang University. In 2011, he joined the School of Electronic and Information, Beihang University, as a Lecturer. His main research interests include microwave/millimeter-wave imaging system design and image processing.

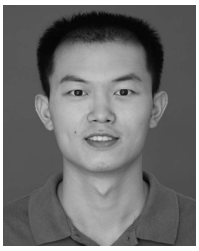

JIANHAO GONG received the B.S. degree from the College of Electronic and Information Engineering, Nanhang University, Nanjing, China, in 2014, and the M.S. degree from Lanzhou University, Lanzhou, China, in 2018. He is currently pursuing the Ph.D. degree with the School of Electronics and Information Engineering, Beihang University, Beijing, China. His current research interests include monolithic microwave integrated circuits design based on gallium arsenide, RF/microwave circuits design, and microwave imaging techniques.

RUOCHEN GU received the B.S. degree from the Beijing Institute of Technology, Beijing, China, in 2017, and the M.S. degree from the National Institute of Metrology, Beijing, in 2020. He is currently pursuing the Ph.D. degree with Beihang University, Beijing. His current research interests include microwave receiver module design and phase-array antenna mutual coupling research.

WANGDONG HE was born in Hubei, China, in 1993. He received the B.S. and M.S. degrees in electromagnetic field and microwave technology from the University of Electronic Science and Technology of China (UESTC), Chengdu, China, in 2015 and 2018, respectively. He is currently pursuing the Ph.D. degree in electromagnetic field and microwave technology with Beihang University, Beijing, China. His current research interests include monolithic microwave integrated circuits design based on gallium arsenide, RF/microwave circuits design, and microwave imaging techniques.

JUNGANG MIAO was born in Shijiazhuang, Hebei, China, in 1963. He received the B.S.E.E. degree from the National University of Defense Technology, Changsha, China, in 1982, the M.S.E.E. degree from Beihang University (BUAA), Beijing, China, in 1987, and the Dr.Rer.Nat. degree in physics from the University of Bremen, Bremen, Germany, in 1998. From 1982 to 1984, he was with the Institute of Remote Sensing Instrumentation, Chinese Aerospace, Beijing, where he was involved in the development of space-borne microwave remote-sensing instruments. From 1984 to 1993, he was with the Electromagnetic Laboratory, BUAA, where he was involved in research and teaching in the field of microwave remote sensing. In 1993, he joined the Institute of Environmental Physics, University of Bremen, as a Staff Member, doing researches on space-borne microwave radiometers. In 2003, he returned to BUAA, where he has been the Chair Professor with the Electromagnetic Laboratory, since 2004. His research interests include electromagnetic wave scattering, microwave and millimeter-wave circuits, and microwave remote sensing instrumentation, including sensor development, calibration, and data processing.